



Terahertz photoresponse of black phosphorus

EDWARD LEONG,¹ RYAN J. SUESS,^{1,2} ANDREI B. SUSHKOV,³ H. DENNIS DREW,³ THOMAS E. MURPHY,^{1,2} AND MARTIN MITTENDORFF^{2,*}

¹Department of Electrical and Computer Engineering, University of Maryland, College Park, MD 20742, USA

²Institute for Research in Electronics and Applied Physics, University of Maryland, College Park, MD 20742, USA

³Center for Nanophysics and Advanced Materials, University of Maryland, College Park, MD 20742, USA

*martin@mittendorff.email

Abstract: Two-dimensional black phosphorus is a new material that has gained widespread interest as an active material for optoelectronic applications. It features high carrier mobility that allows for efficient free-carrier absorption of terahertz radiation, even though the photon energy is far below the bandgap energy. Here we present an efficient and ultrafast terahertz detector, based on exfoliated multilayer flakes of black phosphorus. The device responsivity is about 1 mV/W for a 2.5 THz beam with a diameter of 200 μm , and is primarily limited by the small active area of the device in comparison to the incident beam area. The intrinsic responsivity is determined by Joule heating experiments to be about 44 V/W, which is in agreement with predictions from the Drude conductivity model. Time resolved measurements at a frequency of 0.5 THz reveal an ultrafast response time of 20 ps, making black phosphorus a candidate for high performance THz detection at room temperature.

© 2017 Optical Society of America

OCIS codes: (040.2235) Far infrared or terahertz; (230.0040) Detectors.

References and links

1. P. W. Bridgman, "Two new modifications of phosphorus," *J. Am. Chem. Soc.* **36**(7), 1344–1363 (1914).
2. A. Castellanos-Gomez, L. Vicarelli, E. Prada, J. O. Island, K. L. Narasimha-Acharya, S. I. Blanter, D. J. Groenendijk, M. Buscema, G. A. Steele, J. V. Alvarez, H. W. Zandbergen, J. J. Palacios, and H. S. J. van der Zant, "Isolation and characterization of few-layer black phosphorus," *2D Materials* **1**, 025001 (2014).
3. S. P. Koenig, R. A. Doganov, H. Schmidt, A. H. Castro Neto, and B. Özyilmaz, "Electric field effect in ultrathin black phosphorus," *Appl. Phys. Lett.* **104**(10), 103106 (2014).
4. Y. Wang, G. Xu, Z. Hou, B. Yang, X. Zhang, E. Liu, X. Xi, Z. Liu, Z. Zeng, W. Wang, and G. Wu, "Large anisotropic thermal transport properties observed in bulk single crystal black phosphorus," *Appl. Phys. Lett.* **108**(9), 092102 (2016).
5. F. Xia, H. Wang, and Y. Jia, "Rediscovering black phosphorus as an anisotropic layered material for optoelectronics and electronics," *Nat. Commun.* **5**, 4458 (2014).
6. X. Wang, A. M. Jones, K. L. Seyler, V. Tran, Y. Jia, H. Zhao, H. Wang, L. Yang, X. Xu, and F. Xia, "Highly anisotropic and robust excitons in monolayer black phosphorus," *Nat. Nanotechnol.* **10**(6), 517–521 (2015).
7. V. Tran, R. Soklaski, Y. Liang, and L. Yang, "Layer-controlled band gap and anisotropic excitons in few-layer black phosphorus," *Phys. Rev. B* **89**(23), 235319 (2014).
8. M. Buscema, D. J. Groenendijk, S. I. Blanter, G. A. Steele, H. S. J. van der Zant, and A. Castellanos-Gomez, "Fast and broadband photoresponse of few-layer black phosphorus field-effect transistors," *Nano Lett.* **14**(6), 3347–3352 (2014).
9. N. Youngblood, C. Chen, S. J. Koester, and M. Li, "Waveguide-integrated black phosphorus photodetector with high responsivity and low dark current," *Nat. Photonics* **9**, 247–252 (2015).
10. M. Huang, M. Wang, C. Chen, Z. Ma, X. Li, J. Han, and Y. Wu, "Broadband black-phosphorus photodetectors with high responsivity," *Adv. Mater.* **28**(18), 3481–3485 (2016).
11. R. J. Suess, E. Leong, J. L. Garrett, T. Zhou, R. Salem, J. N. Munday, T. E. Murphy, and M. Mittendorff, "Mid-infrared time-resolved photoconduction in black phosphorus," *2D Materials* **3**, 041006 (2016).
12. L. Viti, J. Hu, D. Coquillat, W. Knap, A. Tredicucci, A. Politano, and M. S. Vitiello, "Black phosphorus terahertz photodetectors," *Adv. Mater.* **27**(37), 5567–5572 (2015).
13. L. Viti, J. Hu, D. Coquillat, A. Politano, W. Knap, and M. S. Vitiello, "Efficient Terahertz detection in black-phosphorus nano-transistors with selective and controllable plasma-wave, bolometric and thermoelectric response," *Sci. Rep.* **6**(1), 20474 (2016).

14. L. Wang, C. Liu, X. Chen, J. Zhou, W. Hu, X. Wang, J. Li, W. Tang, A. Yu, S.-W. Wang, and W. Lu, "Toward sensitive room-temperature broadband detection from infrared to terahertz with antenna-integrated black phosphorus photoconductor," *Adv. Funct. Mater.* **27**(7), 1604414 (2017).
15. Y. Huo, G. W. Taylor, and R. Bansal, "Planar log-periodic antennas on extended hemispherical silicon lenses for millimeter/submillimeter wave detection applications," *Int. J. Infrared Millim. Waves* **23**(6), 819–839 (2002).
16. J.-S. Kim, Y. Liu, W. Zhu, S. Kim, D. Wu, L. Tao, A. Dodabalapur, K. Lai, and D. Akinwande, "Toward air-stable multilayer phosphorene thin-films and transistors," *Sci. Rep.* **5**(1), 8989 (2015).
17. Y. Y. Illarionov, M. Waltl, G. Rzepa, J.-S. Kim, S. Kim, A. Dodabalapur, D. Akinwande, and T. Grasser, "Long-term stability and reliability of black phosphorus field-effect transistors," *ACS Nano* **10**(10), 9543–9549 (2016).
18. Q. Wei, J. He, S. Yang, H. Jia, Y. Liu, W. Liu, Y. Liu, and T. Li, "Investigation of black phosphorus field-effect transistors and its stability," *Opt. Quantum Electron.* **48**(6), 344 (2016).
19. J. Na, Y. T. Lee, J. A. Lim, D. K. Hwang, G.-T. Kim, W. K. Choi, and Y.-W. Song, "Few-layer black phosphorus field-effect transistors with reduced current fluctuation," *ACS Nano* **8**(11), 11753–11762 (2014).
20. N. Gillgren, D. Wickramaratne, Y. Shi, T. Espiritu, J. Yang, J. Hu, J. Wei, X. Liu, Z. Mao, K. Watanabe, T. Taniguchi, M. Bockrath, Y. Barlas, R. K. Lake, and C. N. Lau, "Gate tunable quantum oscillations in air-stable and high mobility few-layer phosphorene heterostructures," *2D Mater.* **2**, 011001 (2015).
21. S. Liu, N. Huo, S. Gan, Y. Li, Z. Wei, B. Huang, J. Liu, J. Li, and H. Chen, "Thickness-dependent Raman spectra, transport properties and infrared photoresponse of few-layer black phosphorus," *J. Mater. Chem. C Mater. Opt. Electron. Devices* **3**(42), 10974–10980 (2015).
22. L. Li, Y. Yu, G. J. Ye, Q. Ge, X. Ou, H. Wu, D. Feng, X. H. Chen, and Y. Zhang, "Black phosphorus field-effect transistors," *Nat. Nanotechnol.* **9**(5), 372–377 (2014).
23. T. Hong, B. Chamlagain, W. Lin, H.-J. Chuang, M. Pan, Z. Zhou, and Y.-Q. Xu, "Polarized photocurrent response in black phosphorus field-effect transistors," *Nanoscale* **6**(15), 8978–8983 (2014).
24. H. Yuan, X. Liu, F. Afshinmanesh, W. Li, G. Xu, J. Sun, B. Lian, A. G. Curto, G. Ye, Y. Hikita, Z. Shen, S.-C. Zhang, X. Chen, M. Brongersma, H. Y. Hwang, and Y. Cui, "Polarization-sensitive broadband photodetector using a black phosphorus vertical p-n junction," *Nat. Nanotechnol.* **10**(8), 707–713 (2015).
25. J. Wu, G. K. W. Koon, D. Xiang, C. Han, C. T. Toh, E. S. Kulkarni, I. Verzhbitskiy, A. Carvalho, A. S. Rodin, S. P. Koenig, G. Eda, W. Chen, A. H. Neto, and B. Özyilmaz, "Colossal ultraviolet photoresponsivity of few-layer black phosphorus," *ACS Nano* **9**(8), 8070–8077 (2015).
26. X. Cai, A. B. Sushkov, R. J. Suess, M. M. Jadidi, G. S. Jenkins, L. O. Nyakiti, R. L. Myers-Ward, S. Li, J. Yan, D. K. Gaskill, T. E. Murphy, H. D. Drew, and M. S. Fuhrer, "Sensitive room-temperature terahertz detection via the photothermoelectric effect in graphene," *Nat. Nanotechnol.* **9**(10), 814–819 (2014).
27. N. M. Gabor, J. C. W. Song, Q. Ma, N. L. Nair, T. Taychatanapat, K. Watanabe, T. Taniguchi, L. S. Levitov, and P. Jarillo-Herrero, "Hot carrier-assisted intrinsic photoresponse in graphene," *Science* **334**(6056), 648–652 (2011).
28. M. W. Graham, S.-F. Shi, D. C. Ralph, J. Park, and P. L. McEuen, "Photocurrent measurements of supercollision cooling in graphene," *Nat. Phys.* **9**(2), 103–108 (2012).
29. F. Xia, T. Mueller, R. Golizadeh-Mojarad, M. Freitag, Y. M. Lin, J. Tsang, V. Perebeinos, and P. Avouris, "Photocurrent imaging and efficient photon detection in a graphene transistor," *Nano Lett.* **9**(3), 1039–1044 (2009).
30. M. Mittendorff, S. Winnerl, J. Kamann, J. Eroms, D. Weiss, H. Schneider, and M. Helm, "Ultrafast graphene-based broadband THz detector," *Appl. Phys. Lett.* **103**(2), 021113 (2013).
31. M. Mittendorff, J. Kamann, J. Eroms, D. Weiss, C. Drexler, S. D. Ganichev, J. Kerbusch, A. Erbe, R. J. Suess, T. E. Murphy, S. Chatterjee, K. Kolata, J. Ohser, J. C. König-Otto, H. Schneider, M. Helm, and S. Winnerl, "Universal ultrafast detector for short optical pulses based on graphene," *Opt. Express* **23**(22), 28728–28735 (2015).
32. Y. Liu, T. Low, and P. P. Ruden, "Mobility anisotropy in monolayer black phosphorus due to scattering by charged impurities," *Phys. Rev. B* **93**(16), 165402 (2016).
33. T. Low, A. S. Rodin, A. Carvalho, Y. Jiang, H. Wang, F. Xia, and A. H. Castro Neto, "Tunable optical properties of multilayer black phosphorus thin films," *Phys. Rev. B* **90**(7), 075434 (2014).
34. T. Low, M. Engel, M. Steiner, and P. Avouris, "Origin of photoresponse in black phosphorus phototransistors," *Phys. Rev. B* **90**(8), 081408 (2014).
35. Y. Saito, T. Iizuka, T. Koretsune, R. Arita, S. Shimizu, and Y. Iwasa, "Gate-tuned thermoelectric power in black phosphorus," *Nano Lett.* **16**(8), 4819–4824 (2016).
36. E. Flores, J. R. Ares, A. Castellanos-Gomez, M. Barawi, I. J. Ferrer, and C. Sánchez, "Thermoelectric power of bulk black-phosphorus," *Appl. Phys. Lett.* **106**(2), 022102 (2015).
37. K. Li, K.-W. Ang, Y. Lv, and X. Liu, "Effects of Al₂O₃ capping layers on the thermal properties of thin black phosphorus," *Appl. Phys. Lett.* **109**(26), 261901 (2016).
38. S. Li, G. Kumar, and T. E. Murphy, "Terahertz nonlinear conduction and absorption saturation in silicon waveguides," *Optica* **2**(6), 553–557 (2015).
39. J. Hebling, G. Almási, I. Kozma, and J. Kuhl, "Velocity matching by pulse front tilting for large area THz-pulse generation," *Opt. Express* **10**(21), 1161–1166 (2002).
40. R. J. Suess, M. M. Jadidi, T. E. Murphy, and M. Mittendorff, "Carrier dynamics and transient photobleaching in thin layers of black phosphorus," *Appl. Phys. Lett.* **107**(8), 081103 (2015).

1. Introduction

Black phosphorus (BP) is the most stable phosphorus allotrope and has been known for several decades [1] before it again gained interest in recent years as a material that can be produced in atomically thin layers. Much like graphite, BP consists of layered sheets of atoms held together by the van der Waals forces. Each atomic layer is separated from the next by approximately 0.5 nm and consists of a corrugated hexagonal lattice of phosphorus atoms. While its properties are not promising in bulk crystals, it can be exfoliated to two-dimensional flakes [2] that can be electrostatically gated to control carrier density [3]. In contrast to graphene and many other 2D materials, its properties like thermal conductivity [4], carrier mobility [5], and optical absorption [6], are highly anisotropic due to the corrugated structure of each layer. Its band gap depends on the thickness of the flake, so while a single layer of BP is characterized by a direct band gap of about 2 eV, the band gap decreases to its bulk value of about 0.3 eV within about 10 atomic layers [7]. Near- and mid-infrared detection in BP has been successfully demonstrated by several groups, proving superior sensitivity and speed compared to most other 2D materials [8–11]. Even though the band gap of 0.3 eV does not allow for direct electron-hole pair excitation in the THz regime, its high mobility allows for THz detection in nano-transistors [12,13]. A very recent study by Wang et al. [14] demonstrates photoconductive detection in the microwave frequency range with a bandwidth of several kHz. Here we study the THz photoresponse of thin flakes of BP at room temperature. The BP flakes are fabricated by mechanical exfoliation on SiO₂/Si and contacted via a logarithmic periodic antenna [15]. We observed a THz response from the photothermoelectric effect providing a responsivity of 0.9 mV/W as well as a modest bolometric response. The intrinsic responsivity is measured via a Joule heating experiment to be around 44 V/W, which is in good agreement with the expected THz heating by free-carrier absorption. Time resolved measurements with a pulsed THz source show a fast response time of about 20 ps, indicating that BP is a promising material for THz detection.

2. Device fabrication and electrical characterization

The THz devices presented in this study are based on field-effect transistors made from thin flakes of BP, fabricated by mechanical exfoliation from a bulk crystal. To estimate the thickness of the BP flakes, the near-infrared transmission through the flake was measured at a wavelength of 1.56 μm . Assuming 2.8% absorption per layer [2], the flakes used for sample fabrication consist of 20 to 80 layers. Although the responsivity varied depending on the flake size, shape, orientation and thickness, we observed a photodetected signal under THz excitation with samples of different thickness, indicating that the thickness is not of major importance. The substrate consists of lightly doped Si with a resistance of 250 Ωcm , covered by a 300 nm thick layer of SiO₂. Source and drain contacts are made to the flake via a logarithmic-periodic antenna that is patterned by photolithography followed by metal deposition with 10nm/100nm Cr/Au. The antenna has an outer diameter of 1 mm and the BP channel in the center of the antenna has a length and width of 10 μm (cf. Fig. 1). The Fermi energy in the BP flake can be varied with a gate voltage that is applied via the Si substrate. A 100 nm thick layer of Al₂O₃ is deposited on the top by atomic layer deposition to protect the BP film from degradation in atmosphere [16]. Multiple studies verify the efficient prevention of degradation of BP flakes with this method [17,18], and it also serves as passivation layer, further improving the device performance [19]. Alternatively, capping of BP devices with hexagonal boron nitride is a reliable way to prevent the flakes from degradation [20]. The encapsulated samples were extensively measured over several weeks under optical and THz illumination under normal ambient temperature and humidity, and showed no significant visible or performance degradation during this period. The integrity of the BP flakes was verified by Raman measurements in backscattering geometry; we observed three peaks at 364 cm^{-1} , 440 cm^{-1} , and 468 cm^{-1} that are characteristic to BP flakes [2,5,21]. A typical Raman spectrum measured on one of our flakes is presented in Fig. 2(a).

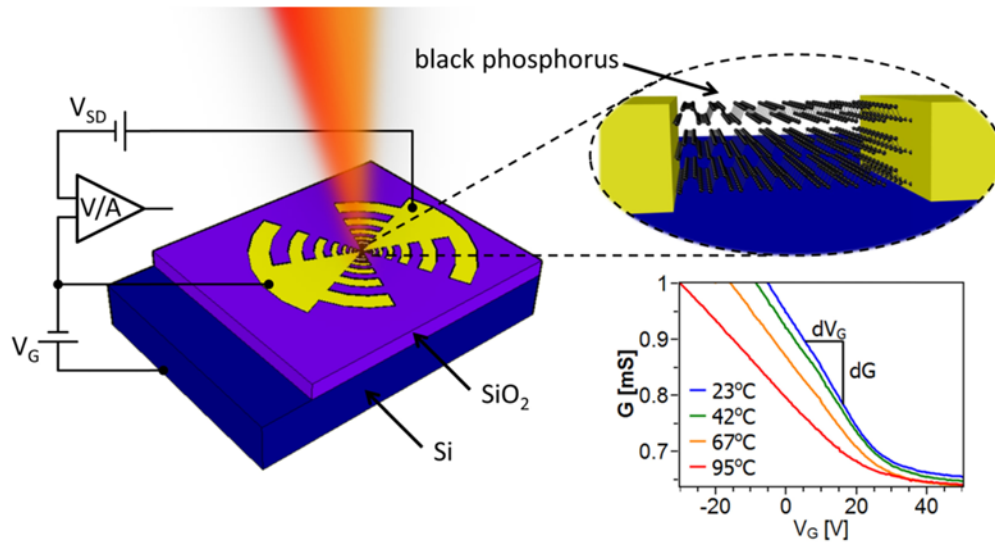


Fig. 1. Sketch of the device structure including the electrical connections. The curves in the lower right part of the figure show the conductivity of the black phosphorus flake as a function of the gate voltage at various temperatures.

The gate curve at various temperatures for a constant source-drain voltage of 0.1 V is shown in the lower right part of Fig. 1. When the gate voltage is absent, transport in the channel is dominated by holes, which have a higher mobility than electrons in BP [22]. From the gating curve, the mobility is estimated as $\mu = \frac{L}{W} \frac{1}{C_g} \frac{dG}{dV_g}$ [15], where $\frac{L}{W}$ represents the aspect ratio of the channel, C_g the capacitance per unit area, G is the conductance of the channel, and V_g is the gate voltage. From the measurements presented in the inset of Fig. 1, the hole mobility μ_h is calculated to be $(870 \pm 70) \text{ cm}^2/(\text{Vs})$. As the flake in this device is rather thick (about 80 layers), the remaining conductivity at the highest gate voltage of 50 V is still high. The presence of residual carriers results in metallic properties, such as a decreased conductivity with increasing temperature. This bolometric effect can be measured as a decrease in conductivity as the device is heated by incident radiation.

3. Experimental results

Due to the corrugations in the crystal lattice, the near infrared absorption and resulting photocurrent depend strongly on the polarization of the incident radiation [23–25]. To determine the orientation of the BP flake, we performed polarization dependent photocurrent measurements with near infrared radiation. An aspherical lens was used to focus the 1.5 μm radiation from a fiber laser to a spot size of approximately 3 μm . The red line in Fig. 2(b) shows the near infrared photocurrent as a function of the polarization angle at a bias voltage of 50 mV. The largest photocurrent is achieved when the radiation is polarized along the high mobility axis, which is perpendicular to the corrugations of the BP. This indicates that the contacts are aligned to about 20° to the high mobility axis.

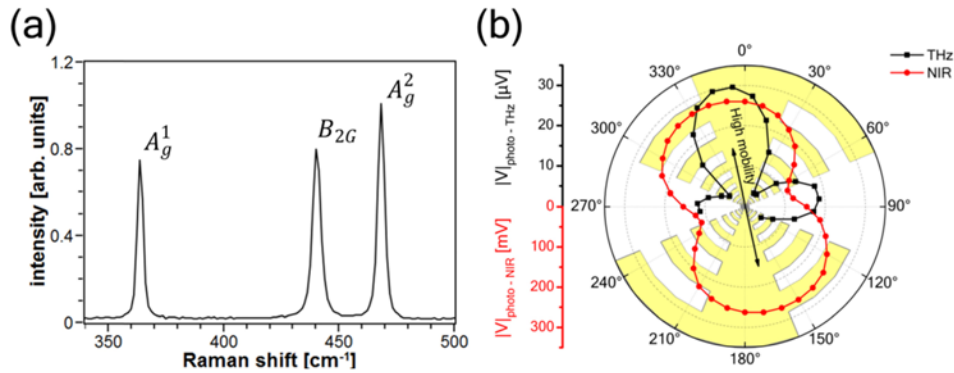


Fig. 2. (a) Raman spectrum of a typical flake of black phosphorus after Al_2O_3 deposition. (b) Polarization dependence of the photovoltage measured at $1.55 \mu\text{m}$ (red) and $120 \mu\text{m}$ (black). The yellow shape in the background represents the logarithmic-periodic antenna.

To characterize the THz response of the device, we employed a CW methanol gas laser at a frequency of 2.5 THz. The beam intensity was modulated with a mechanical chopper at a frequency of 50 Hz to enable lock-in detection; a half wave plate in the beam path was used to control the polarization orientation of the THz radiation. An off-axis parabolic mirror was used to focus the THz radiation with a power of 6 mW to a spot size of about $200 \mu\text{m}$. To read out the photoresponse from the BP, the device is connected to a lock-in amplifier via a transimpedance amplifier that also provides a source-drain bias voltage. The polarization dependent THz response is measured at a bias voltage of 0 mV and a gate voltage of 5 V and is shown as a black line in Fig. 2(b). At 2.5 THz the response exhibits a larger variation with polarization angle than the near infrared photosignal (red line Fig. 2(b)). Maximum THz signals are observed when the light is polarized along the high mobility axis of the BP flake and is caused by free-carrier absorption, which depends explicitly on the mobility of the carriers. The differences between the THz and near infrared signals are consistent with prior observations that show the carrier mobility anisotropy to be more pronounced than the interband absorption anisotropy (cf., Fig. 2(b) in Ref [5]). The second peak in the THz response at 80° corresponds to the optimum coupling polarization angle of the antenna. The $1 \text{ k}\Omega$ resistance of BP channel limits the coupling between the flake and the antenna, which is designed for an impedance of 50Ω .

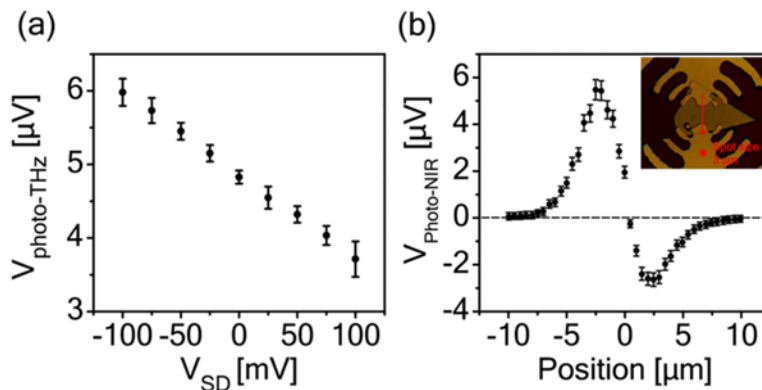


Fig. 3. (a) Photocurrent measured at 2.5 THz as a function of the applied source-drain bias. (b) Photocurrent measured at a wavelength of $1.55 \mu\text{m}$ as a function of the focus position in the black phosphorus channel (cf. inset).

To further investigate the origin of the THz photo response, we measured the photovoltage as a function of the gate voltage (not shown) and as a function of the source-drain bias (cf. Fig. 3(a)). The highest photovoltage is achieved at positive gate voltage, when the conductivity is minimized. This behavior is similar to the photothermoelectric response observed in graphene devices [24]. At lower gate voltages, the signal decreases moderately by about 10%. Varying the source-drain bias at a fixed gate voltage leads to a linear change of the measured signal, which is caused by a bolometric effect: as the THz radiation heats the flake, the conductivity decreases as observed in the gate curves at different temperatures presented in Fig. 1(b). At zero bias, the photo response exhibits a 5 μV signal that cannot be explained by a bolometric response, which is expected to be zero when no source-drain voltage is applied. To further investigate the origin of this photovoltaic response, we performed I/V measurements in which the source-drain current is monitored as a function of the bias voltage. These measurements show a perfect proportionality between source-drain current and voltage, which excludes a photo voltage from Schottky barriers at the contacts. Another possible photosignal that will be present without applied source-drain voltage is the photothermoelectric effect [26]. A temperature gradient within the BP channel leads to a charge transfer between the contacts, causing the photovoltage. Such a temperature gradient can be achieved by local gating [27,28], local excitation [29], or dissimilar metals for the contacts [24]. In the present work, asymmetric heating and diffusion is caused by the irregular shape of the exfoliated BP flake and the imbalance between the source and drain contact regions formed between the antenna and flake. A tightly focused near-infrared beam at a wavelength of 1.56 μm was used to further investigate the asymmetry of the device by measuring the photovoltage as a function of the spatial position of the near-infrared beam across the center of the device channel. The result of this measurement is shown in Fig. 3 (b). When the radiation is focused on the upper contact, a positive photocurrent is measured, illuminating the lower contact leads to a negative photocurrent. For a symmetric device, these two contributions would cancel when both contacts are equally illuminated, as with the THz radiation. As the positive peak is stronger than the negative one, a net positive current is produced even under uniform illumination. From the CW THz measurements we estimate the maximum overall responsivity of about 1 mV/W, which is more than one order of magnitude higher than similar devices based on graphene [30,31]. The noise equivalent power (NEP) of our device is measured to be 130 $\mu\text{W}/\text{Hz}^{0.5}$ and has the potential to be further reduced to the temperature limited NEP of 4.5 $\mu\text{W}/\text{Hz}^{0.5}$ if electrical shielding of the device is employed to reduce coupling to the wiring of the device.

Measuring the intrinsic responsivity produced by the photothermoelectric effect in our device requires knowledge of both the THz-antenna coupling and the impedance mismatch between the antenna and BP flake. A direct measure of the intrinsic responsivity can be achieved without this information, however, by instead heating the flake electrically via Joule heating [26]. When the device is electrically heated by applying an AC current with frequency ω , the resulting voltage exhibits (in addition to the ohmic contribution) a small DC and 2ω contribution caused by the thermoelectric effect. The 2ω contribution is measured with high sensitivity using lock-in detection. The circuit diagram of the measurement setup is shown in the inset in Fig. 4(a). The voltage drop over the BP device is given by $v = iR + \alpha iv$, where αiv represents the thermoelectric signal that is the product of the responsivity α and the absorbed power iv . Because $\alpha i \ll 1$, the voltage can be approximated by $v = iR + \alpha Ri^2$. The current in this circuit is limited by the resistor R_0 that is about 100 times larger than the device resistivity. Hence, the current through the device can be approximated by $i(t) \approx \frac{V_0}{R_0} \cos(\omega t)$. The voltage drop over the device is described by

$$v(t) = \frac{v_0}{R_0} R \cdot \cos(\omega t) + \alpha \frac{R v_0^2}{2R_0^2} [1 + \cos(2\omega t)]. \quad (1)$$

In addition to the conventional ohmic term, the voltage includes a thermoelectric contribution proportional to the electrical power $P(t) = \frac{R v_0^2}{2R_0^2} [1 + \cos(2\omega t)]$. For a sensitive measurement of the thermoelectric signal we apply an ac voltage with a frequency of 5 kHz, and measure the Fourier component at 10 kHz using a lock-in amplifier. As shown in Fig. 4(a), the measured thermoelectric voltage is proportional to the electrical power, from which we estimate an intrinsic thermoelectric responsivity of $\alpha = 44$ V/W. Power dependent measurements at 2.5 THz show a similar proportionality between the measured signal and the applied THz power (cf. Figure 4(b)), corresponding to an overall responsivity of 0.9 mV/W.

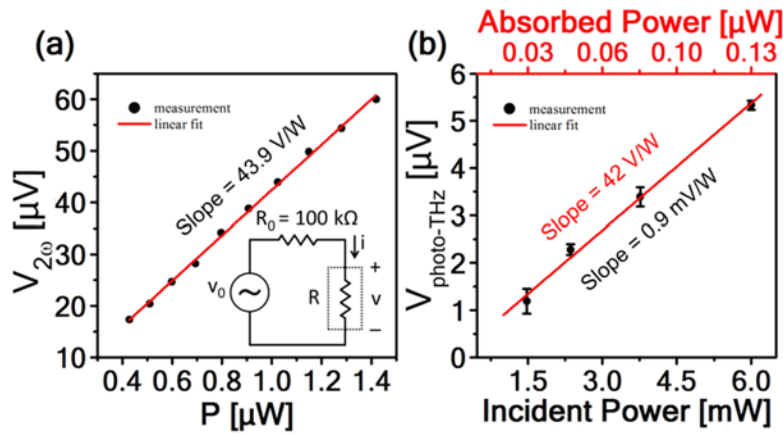


Fig. 4. (a) Photothermoelectric voltage generated in the black phosphorus flake as a function of the electrical power. The inset shows the schematic of the measurement setup to determine the intrinsic responsivity. (b) Photovoltage as a function of the incident THz power (lower axis), the red axis shows the estimated absorbed power via the Drude model.

To compare this intrinsic responsivity to our THz measurements, we estimate the free-carrier absorption in the BP flake. We assumed free-carrier absorption that was calculated via Drude model to be $\sigma(\omega) = \frac{\sigma_{dc}}{1 + i\omega\tau}$, where σ_{dc} represents the dc conductivity that was extracted from the gate curve in Fig. 1(a). The momentum scattering time τ was assumed to be 200 fs, which is consistent with theoretical predictions [32]. The reflectivity can be estimated using the complex conductivity by $r = -\frac{\epsilon_0 c \sqrt{\epsilon_{Si} - \epsilon_{air}} + \sigma(\omega)}{\epsilon_0 c \sqrt{\epsilon_{Si} + \epsilon_{air}} + \sigma(\omega)}$. In this expression c is the speed of light in vacuum, ϵ_0 is the vacuum permittivity, ϵ_{Si} and ϵ_{air} are the relative permittivities of silicon and air, respectively. The absorption coefficient is calculated via the relation $\alpha = 1 - R - T$, where $R = |r|^2$, and $T = 1 + |r|^2 \sqrt{\epsilon_{Si} - \epsilon_{air}}$ [33], to be about 0.7%. From the channel geometry ($A_{Dev} = 100 \mu\text{m}^2$) and the spot size of the THz beam ($A_{Spot} = 31,000 \mu\text{m}^2$), we estimate the maximum absorbed power via $P_{abs} = \alpha P_{THz} \frac{A_{Dev}}{A_{Spot}}$ to be 0.13 μW . The numbers at the upper axis in Fig. 4(b) represent the calculated absorbed power. In terms of the absorbed power, we estimate a responsivity of 42 V/W which is in good

agreement with the intrinsic responsivity of 44 V/W which was determined by Joule heating measurements. In terms of the absorbed power, this intrinsic responsivity corresponds to a NEP of around 100 pW/Hz^{1/2}.

The electrical characterization at various temperatures allows us to theoretically calculate the THz response of our device: from the gate dependence shown in Fig. 1, we can estimate the Seebeck coefficient of our device via the Mott formula [33]:

$$S = \frac{-\pi^2 k_B^2 T}{3C_{Ox}} \left(\frac{1}{\sigma} \frac{d\sigma}{dV_g} \right) \frac{dn}{dE_F}. \quad (2)$$

Here, k_B represents the Boltzmann constant, T the temperature, C_{Ox} is the gate capacitance for a 300 nm thick SiO₂, σ the conductivity, and V_g is the gate voltage. The carrier density $\frac{dn}{dE_F}$ for multilayer BP is estimated within the effective mass framework [31].

With this, we estimate a Seebeck coefficient of about $-130 \mu\text{V/K}$, which is in the range of previously reported values [14,34–36]. To reach a thermoelectric signal of about 5 μV , the temperature variation within the channel has to be about 40 mK. Assuming an exponential decay over the channel, we estimate an average temperature increase of about 8 mK. Li et al. investigated the thermal properties of BP flakes that are capped by Al₂O₃ by power dependent Raman measurements [37]. From their observation we can estimate a temperature increase of about 14 mK if 0.1 μW is absorbed in the flake, which is close to the 8 mK that we derived from the Seebeck coefficient. For an average temperature increase of 8 mK, we can derive the bolometric signal at an applied bias of 100 mV from the gate curves at various temperatures to be 1.3 μV . This value closely matches the measured value of 1.2 μV , supporting our assumptions about the mechanisms of the THz response. In contrast to our observations, Wang et al. have reported an additional decrease in conductivity that is stronger than what is expected from a purely bolometric response. They attribute this effect to electrons from the metal–BP interface that deplete the hole gas [14].

The bandwidth of the detector is characterized using 1 ps wide THz pulses generated by optical rectification of ultrafast optical pulses (800 nm pulses with 40 fs pulse width and 1 kHz repetition rate) in a LiNbO₃ crystal [38,39] (cf. Fig. 5(a)). The THz radiation was focused to a spot size of about 1 mm with a polymethylpentene (TPX) lens to the BP device which was covered with a Si window to block any scattered 800 nm pump light. The signal was recorded with a sampling oscilloscope with a bandwidth of 40 GHz at three different pulse energies.

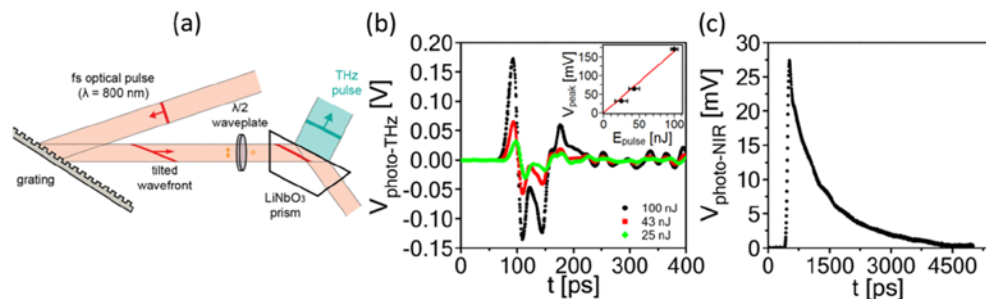


Fig. 5. (a) Sketch of the setup for the THz pulse generation. (b) Time resolved measurement of the photovoltage signal obtained at a frequency of 0.5 THz and a pulse duration of about 1 ps. (c) Time resolved signal obtained at a wavelength of 1.55 μm .

These measurements reveal an ultrafast THz response as shown in Fig. 5(b). The signal is characterized by a short positive peak with a duration of about 30 ps followed by about 200

ps of ringing. The linearity of the pulsed photosignal is measured by attenuating the 100 nJ pulses with Si wafers to obtain lower pulse energies of 43 nJ and 25 nJ. The peak scales linearly with the applied pulse energy and no saturation was observed (see Fig. 5(b) inset). Notably, the delay of the peak for lower pulse energies is not an artifact, but is caused by the transit time through the Si wafers (4 ps per wafer). Figure 5(c) shows the photoconductive response of the device when excited with an ultrashort pulse at a wavelength of 1.55 μm . While the temporal response of BP devices in the near-infrared range is mostly dominated by the 1 ns recombination time of photoexcited carriers [11,40], no additional carriers are generated by THz radiation since the photon energy is far below the BP bandgap. The temporal response is instead limited by the momentum relaxation time of carriers heated by the THz radiation, indicating that response times exceeding those based on carrier recombination lifetimes can be expected from BP detectors operating in the THz regime.

The ultrafast response of the photothermoelectric effect in BP is a promising approach for THz detection. To enhance the performance of the BP THz detector, the geometry of the channel in the center of the antenna should be optimized: Decreasing the channel length to 1 μm and increasing the width to about 20 μm would decrease the resistivity to about 50 Ω , which enables impedance-matching between the antenna and the BP flake. Conversely, the input impedance of the antenna could be controlled through the antenna geometry to match that of the BP channel. Further enhancement of the photothermoelectric effect is possible by using dissimilar metals for the two arms of the antenna to tailor the thermopower coefficient across the BP channel. The difference in the work function of the two metals, e.g. Au and Cr, leads to a different Fermi energy pinning in the BP flake at the contacts, and results in an asymmetric Fermi energy profile [24]. This asymmetry leads to an enhancement of the Seebeck coefficient and maximizes the responsivity of the BP device. Using dissimilar metals will increase the intrinsic responsivity beyond the 44 V/W reported here while an optimized gate geometry will improve the coupling of the THz radiation to the device.

4. Conclusion

We demonstrated an ultrafast THz detector based on exfoliated flakes of BP. The high mobility of nearly 1000 $\text{cm}^2/(\text{Vs})$ enables free-carrier absorption in the far-infrared range and a fast response limited by a carrier scattering. The photothermoelectric effect is found to be the primary source of the THz photosignal and Joule heating experiments demonstrated an intrinsic responsivity of about 44 V/W that is consistent with the observed THz response. Further optimizing the channel geometry and using dissimilar metal contacts to improve the intrinsic responsivity will improve the device performance.

Funding

Office of Naval Research (ONR) (N000141310865); National Science Foundation (NSF) Award No. ECCS1309750.

Acknowledgments

The sample fabrication was carried out at the University of Maryland Nanocenter.